Chapter 6

Plasmonic Au-Ag Bimetallic Nanoporous Film as Flexible SERS Substrate for Detection of Molecular Level R6G dye and Vitamin B_{12}

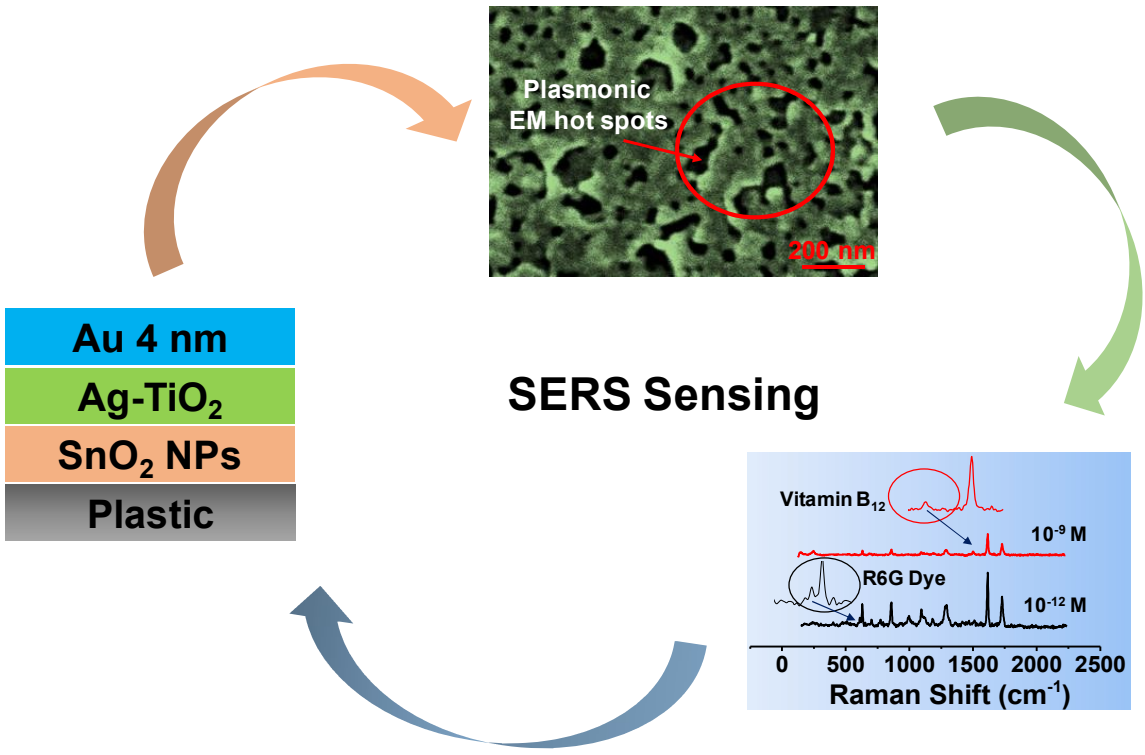

Chapter 6

This chapter also mainly focuses on development of a bimetallic Au-Ag TC film and then used that film for the detection of low molecule via Surface-Enhanced Raman Scattering (SERS) study. It is known that the surface roughness and nanostructures of novel metal thin film plays the major role in SERS study due to their intrinsic EM hotspots, multipolar resonance, and other factors. Based on that knowledge, I developed a low cost and scalable method to fabricate a nano-porous Au-Ag bimetallic thin film on a plastic substrate. This percolated and conducting Au-Ag nanostructured thin film is developed by thermally deposited Au film (4 nm mass thickness) onto a pre-deposited Ag-TiO_2 thin film. This Ag-TiO_2 film, consisting of Ag nanoparticles (NPs) embedded in TiO_2, is grown on SnO_2 nanoparticle (NPs) thin film, forming a nano-porous structure with an average roughness of 3.9 nm. Moreover, this Au-Ag nanostructured is grown inside/over TiO_2 that helps plasmon induced hot electrons transfer from Au-Ag nanostructure to the conduction band of TiO_2, which can enhance the SERS sensitivity of the substrate. This flexible Au (4 nm)/Ag-TiO_2/SnO_2 (NPs) substrate demonstrates efficient SERS-based sensing, detecting Rhodamine 6G (R6G) dye and Vitamin B_{12} down to 1 pM and 1 nM concentrations, respectively. Detailed investigation of the Au (4 nm)/Ag-TiO_2/SnO_2 NPs substrate for R6G detection shows its capability to detection limit up to a single molecule level where as it can detect vitamin B_{12} up to 89 molecules. These observations are attributable due to improved photo induced charge transfer (PICT) processes. This typical porous nature of the bimetallic thin film aids in dispersing the analytes, thus lowering particle density for single molecule optical detection, and enabling low-concentration measurements.

6.1 Introduction

SERS is an efficient analytic technique which amplifies the Raman signal on a metallic nanostructured surface to identify the highly sensitive chemical and biological molecules or structures.[298] This technique enables molecule level detection [263, 299]with an

enhancement factors up to ~10^{13}-10^{14}.[300, 301] Recently, novel metal-based plasmonic NPs such as Au, Ag, Cu have emerged as key players in various scientific and technological fields due to their multifunctional properties, including tunable optical, electrical, and catalytic behaviors.[262, 302-304] These NPs find wide applications in plasmonic photodetectors, photo catalysis, transparent conductor & heat reflector, memory devices, chemical and gas sensing, bio imaging, SERS and so on.[305-309] The size, shape, composition and surrounding medium of these mono-metallic, bimetallic, or multicomponent NPs are the key factors of their plasmonic properties.[310, 311] For SERS substrate application, bimetallic or metal/metal oxide heterostructures are gaining attention for their enhanced optical properties compared to single-metal nanostructures. Particularly, Au-Ag bimetallic nanostructures are gaining interest due to the enhanced plasmonic effect of Ag NPs and superior chemical stability of Au component.[312-315] Advantageously, Ag nano-structures may allow the growth of Au on its surface without alloy formation due to their same set of lattice parameters if processing temperature is restricted <50 °C, leading to the synthesis of bimetallic nanostructures.[316] The growth of Au on Ag leads to the creation of various LSPR, which can be tuned from visible to near-infrared regions, depending on the core Ag geometry and atomic ratio of Ag and Au.[317, 318] This tunability extends the applications of SERS sensing and biomedical fields, especially in NIR regions where background fluorescence is minimal.[319, 320] Instead of the advantages SERS enhancement factors of these Ag-Au based bimetallic plasmonic NPs is limited for practical applications that required further research.

SERS enhancement relies on EM and chemical mechanisms. EM enhancement, the primary component, arises due to the electric field generated on the surface of novel metal nanostructures by excited surface plasmons (SPs), while chemical enhancement involves charge transfer between nanostructures and adsorbed molecules.[321, 322] In both case, analytes required an accessible surface for strong molecule-metal interaction.[323] However, most of the colloidal plasmonic NP synthesis required organic ligands which limit that molecule-metal interaction. Besides, a metal oxide semiconductor contact of plasmonic NP helps light induced hot electron transfer from metal NP to semiconductor that effectively enhances chemical mechanism.[324] Therefore, an ideal SERS system would be ligand free metal NP/metal oxide heterostructure to maximize enhancement factors. However, only few

studies have successfully combined these components into a stable, low-cost, highly sensitive, and flexible SERS substrate.[325, 326] Besides, plasmonic hot electron of novel MNPs can efficiently transfer to a conduction band (CB) of a metal oxide semiconductor like TiO_2.[194, 196] This energy charge transfer (CT) phenomena from metal NPs to the CB of oxide semiconductor can largely improve the enhancement factor of SERS signal.[327, 328] This concept has been explored mostly with the Ag/TiO_2 system due to the strong SPR of Ag and very fast charge transfer from Ag NPs to TiO_2.[329] However, the environmental stability of Ag NPs is not that high. Therefore, in-depth research is required to develop a stable metal/metal-oxide SERS substrate with high enhancement factor.

Herein, this study demonstrated the fabrication strategy of environmentally stable and highly sensitive SERS substrate by using Au-Ag bimetallic nanostructured based plasmonic thin film grown on a mechanically flexible plastic substrate. These plasmonic Au-Ag nanostructured is grown in the TiO_2 matrix that improve the enhancement factor of SERS signal by efficient CT phenomena. For this synthesis, 4 nm mass-thickness of Au has been deposited by thermal evaporation on a pre-deposited Ag-TiO_2/SnO_2 NPs thin film which is grown by a low temperature solution processed technique. This Au/Ag-TiO_2/SnO_2 NPs substrate is not only mechanically flexible, but also optically transparent and electrically high conducting. The SERS study has been investigated by using this substrate with R6G dye and vitamin B_{12} biomolecules as analytes, indicating their detection limits of 10^{-12} M and 10^{-9} M, with an enhancement factor of 3.4×10^8 and 2.2×10^5 respectively.

6.2 Experimental Section

6.2.1 Preparation of Precursor Materials

The preparation process for ion-conducting dielectric LTO and SnO_2 NPs via low temperature solution process technique has been explained in **Chapter 2 Section 2.1.1 and 2.1.3.** Preparation method of analytic solution R6G dye and Vitamin B_{12} is reported in **Chapter 2 Section 2.1.12.**

6.2.2 Fabrication of Au-Ag SERS Substrate

Bimetallic Au-Ag based SERS substrate has been fabricated on a flexible PET substrate and the fabrication steps has been explained **Chapter 2 Section 2.3.3**, and schematically present in **Figure 2.9**.

6.3 Results and Discussion

6.3.1 Surface Morphology (HR-SEM & AFM)

The surface morphology of (4 or 6 nm Au)/Ag-TiO_2/SnO_2 NPs thin film is studied by HR-SEM. **Figure 6.1a&b)** demonstrated the morphological change of the films with different mass thickness of thermally deposited Au film over Ag-TiO_2/SnO_2 NPs thin film. At a critical Au deposition, a percolated Au nanostructure formation is observed which is realized from the sudden change of its morphology. At the initial stage of this growth, thin films are composed of metallic Au islands which forms interconnecting paths of Au as growth is progressed and the residual voids are filled up with additional deposition.[330] The percolated growth of Au during thermally grown Au becomes possible due enhanced lateral growth rate of Au which is promoted by the pre-deposited Ag-TiO_2/SnO_2 NPs thin film due to the pre-existing highly dense Ag-NP that works a nucleation point of Au growth. This possible phenomenon has been realized from the Au film growth on a reference clean plastic substrate which is shown in **Figure 5.7a)**. Reference sample clearly show an isolated grain-like Au growth over the plastic substrate upto 10 nm mass thickness, implying the importance of pre-deposited Ag-TiO_2/SnO_2 NPs as an initial layer which helps to reach percolated nano-porous structure at 4 nm Au mass thickness. Moreover, the nano-porous structure of this SERS substrate (**Figure 6.1a)**) can create intrinsic EM hot spots which effectively enhance the sensitivity of the film. Further deposition of Au film (~ 6 nm) covers the voids, results less effective sensitivity which is shown in **Figure 6.1b)**, is used as a reference film to study side by side of the actual film. EDX and color-mapping attached to the HR-SEM instrument is used to figure out the contents and amount of metallic elements present in both type of film 4 nm Au/Ag-TiO_2/ SnO_2 NPs (**Figure 5.5**) and 6 nm Au/Ag-TiO2/SnO2 NPs (**Figure 6.2**) which confirms the presence of Au, Ag, Ti, Sn and O uniformly throughout the thin film.

Further, AFM has been used for more detailed surface study of Au/Ag-TiO_2/SnO_2 NPs thin films to recognize the surface roughness (R_{rms}) in **Figure 6.1c&d)**. Surface roughness for 4 nm Au/Ag-TiO_2/SnO_2 NPs is quite high (R_{rms}~3.91 nm) compared to 6 nm Au/Ag-TiO_2/ SnO_2 NPs (rms~1.62 nm). Besides, 4 nm Au/Ag-TiO_2/SnO_2 NPs film has larger porosity compared to the 6 nm Au/Ag-TiO_2/SnO_2 NPs which is beneficial for generating hotspot and multipolar resonance effect during the interaction with EM wave that essentially enhanced the SERS significantly. The height profile of these two films are shown in the inset of **Fig. Figure 6.1c&d)** whereas **Figure 6.1e&f)** shows the 3-D AFM image of these two respective films.

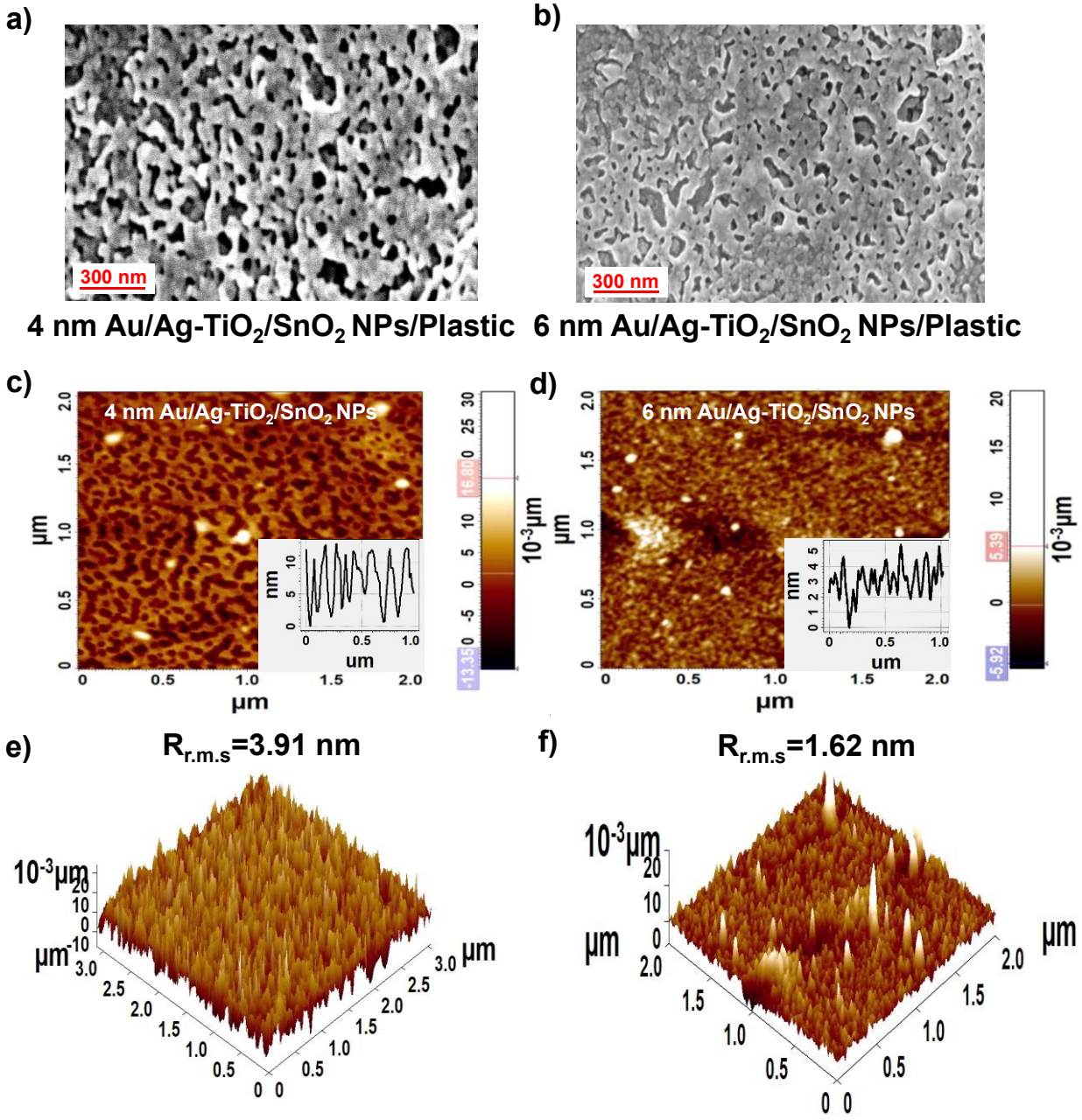

Figure 6.1 FE-SEM photographs of Au/Ag-TiO_2/SnO_2 NPs thin film at room temperature on plastic. Each photograph's average film thickness is listed below. **a)** percolating nano-porous structures **b)** complete percolating structures **c&d)** 2-D AFM image of (4 or 6 nm Au)/Ag-TiO_2/SnO_2 NPs. Each image height profile is listed in the inset **e&f)** 3-D AFM image of (4 or 6 nm Au)/Ag-TiO_2/SnO_2 NPs. R.M.S Roughness of each film is listed in the graphics.

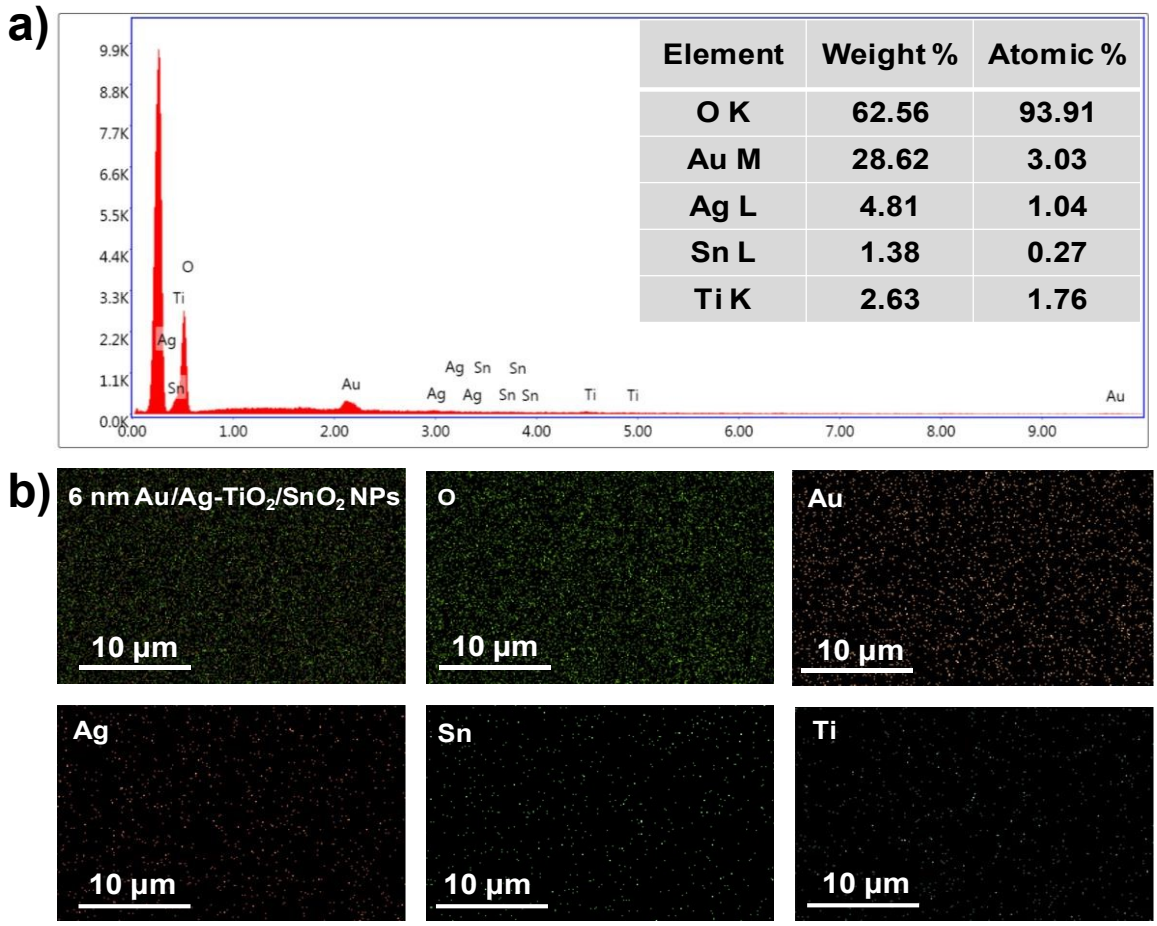

Figure 6.2 EDX and color mapping image of 6 nm Au/Ag-TiO_2/SnO_2 NPs on plastic.

6.3.2 XRD, Raman, UV-Vis Absorption, and PL Spectra

Figure 6.3a) depicts XRD pattern of the thin films that are deposited in the similar way as of Au-Ag based bimetallic nano films fabrication This figure clearly shows the XRD patterns of both substrates (4 or 6 nm Au)/Ag-TiO_2/SnO_2 NPs) exhibits identical XRD pattern but with different intensities. In both cases, the peak position is located at 2θ of 26.17˚, 33.58˚, 51.47˚ and 54.45˚ which corresponds to (110), (101), (211), and (310) planes respectively, indicating the formation of SnO_2 NPs thin film over the substrate (JCPDS file no. 411445). Also, the peak position of TiO_2 at 2θ ~ 24.52˚ corresponds to (110) planes (JCPDS file no. 731764). Besides, the peak position of Au or Ag NPs are located at 2θ ~ 37.83˚ and 44.02˚ which corresponds to (111) and (200) planes respectively (JCPDS file no. 897322). The XRD peak positions of Au or Ag NPs are common because of their very similar lattice parameters.

From this XRD spectra its very clear that the width of the peaks is quite wide, indicating the small size of the metal/metal oxide nanoparticle.

The synthesized 4 nm and 6 nm Au/Ag-TiO_2/SnO_2 NPs thin film are characterized using Raman spectroscopy with 532 nm excitation laser sources. The Raman spectra of both samples, collected using a green laser (532 nm), are displayed in **Figure 6.3b).** The presence of various characteristic phonon modes at ~628 cm^{-1} is arising due to the SnO_2 NPs, at ~ 856,1287 and ~1725 cm^{-1} are observed for plastic substrate, and Raman modes observed at ~1098 & 1613 cm^{-1} are because of Au/Ag NPs. Raman Spectra of reference plastic substrate is given in **Figure 6.4a)**.

For optical studies, thin film of (4 or 6 nm Au)/Ag-TiO_2/SnO_2 NPs is fabricated on a quartz substrate. **Figure 6.3c)** displays the normalized UV-Vis absorbance spectrum of Au/Ag-TiO_2/SnO_2 NPs thin films throughout the optical spectral range of 300–1800 nm. The absorption spectra of as-prepared (4 or 6 nm Au)/Ag-TiO_2/SnO_2 NPs thin films demonstrate strong plasmonic absorption with wide spectral broadening extended from UV-Vis to NIR region up to 1600 nm with a peak position ~ 750 nm. However, reference pure Ag NPs film has a plasmonic peak situated in the blue region around 420-440 nm, while reference Au NPs film has a plasmonic peak of around 520-550 nm. Therefore, it can be concluded that the bimetallic Au-Ag NP formation causes the absorption peak shift to ~750 nm with a large broadening of spectra extended up to 1500 nm, particularly for the longitudinal plasmon mode of this metallic network. The photoluminescence (PL) spectra of the (4 or 6 nm Au)/Ag-TiO_2/SnO_2 NPs thin film is shown in **Figure 6.3d)** which is acquired in the range of 320-550 nm with an excitation wavelength of 300 nm, indicating the emission peaks of around 370 nm (3.35 eV), with a FWHM of 55 nm. The PL peak position at 370 nm suggests specific optical properties that could be attributed to the formation of an Au-Ag NP on TiO_2/SnO_2 matrix. We also observed that the reference pure Au NPs also have PL with the same peak position (~370 nm) but with much lower intensity (**Figure 6.4b)**).

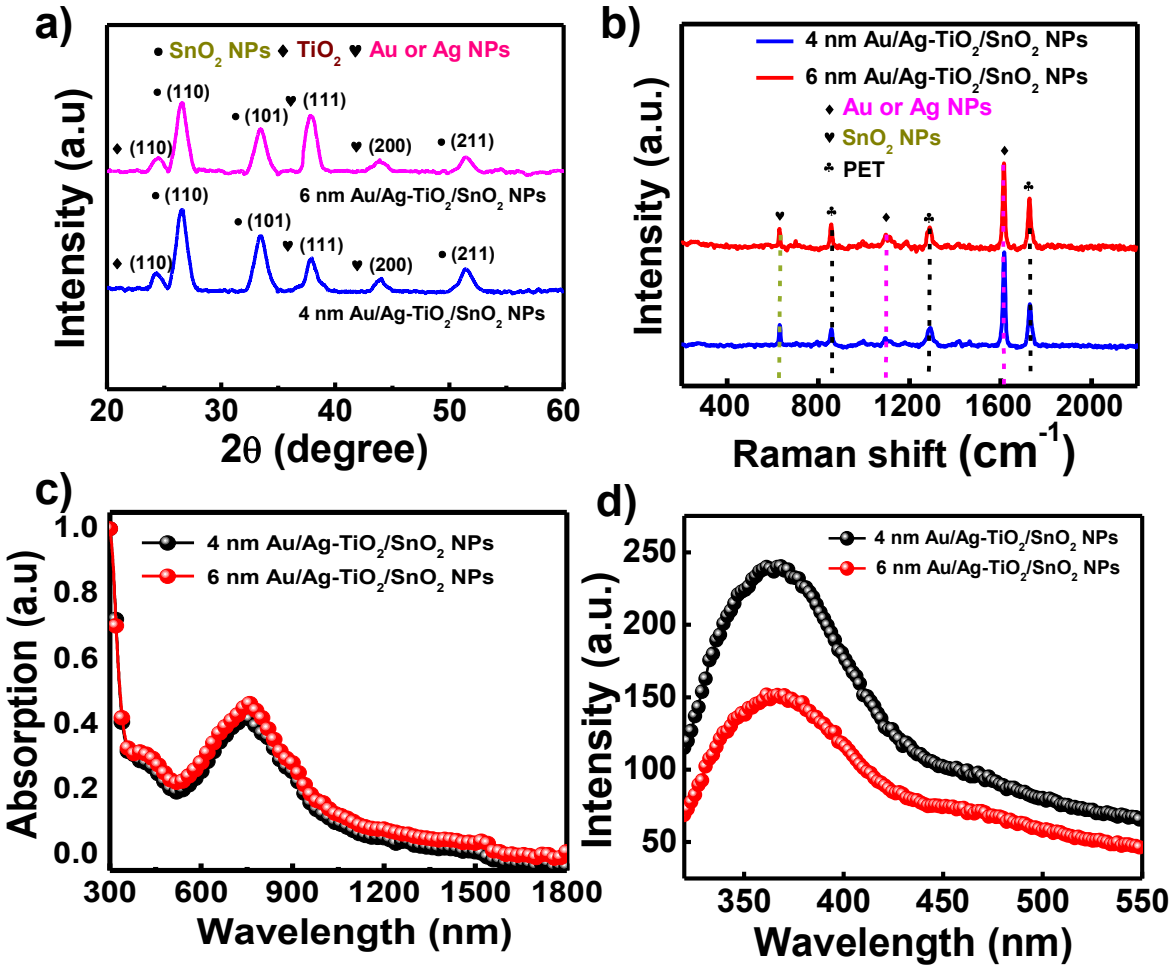

Figure 6.3 structural analysis of (4 or 6 nm Au/Ag-TiO_2/SnO_2 NPs/plastic) **a)** XRD **b)** Raman **c)** UV-Vis **d)** PL spectra.

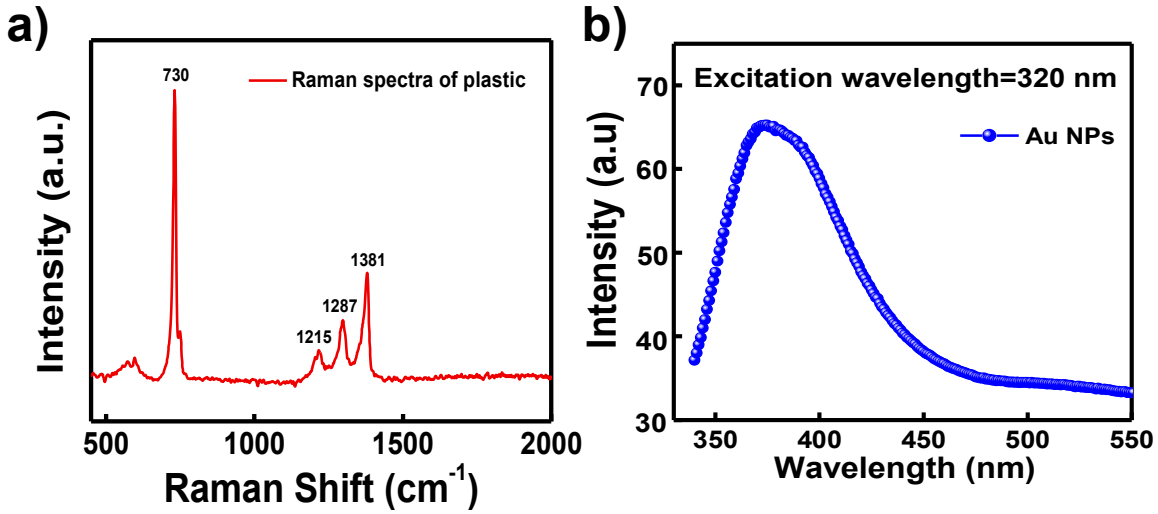

Figure 6.4a) raman spectra of plastic PET **b)** PL spectra of reference 4 nm Au/plastic.

6.3.3 SERS Study

We have performed a SERS study to detect R6G dye using 4 nm and 6 nm Au/Ag-TiO_2/SnO_2 NPs thin films as SERS substrates, which is shown in **Figure 6.5a&b)**. The limit of detection for R6G, adsorbed over 4 nm and 6 nm Au/Ag-TiO_2/SnO_2 NPs thin films substrates are found to be 10^{-12} M and 10^{-9} M, respectively, which is an excellent SERS activity at room temperature. With increasing dye concentrations, the SERS peaks for R6G become more intense. **Figure 6.5c&d)** displays the linear response curve of a prominent peak (~ 611 cm^{-1}) intensity with dye concentration. A notable intensity at picomolar concentration indicates that R6G is highly detectable. The most intense peak, centered around 611 cm^{-1} for R6G dye, is due to the aromatic C-C stretching of the R6G molecule.

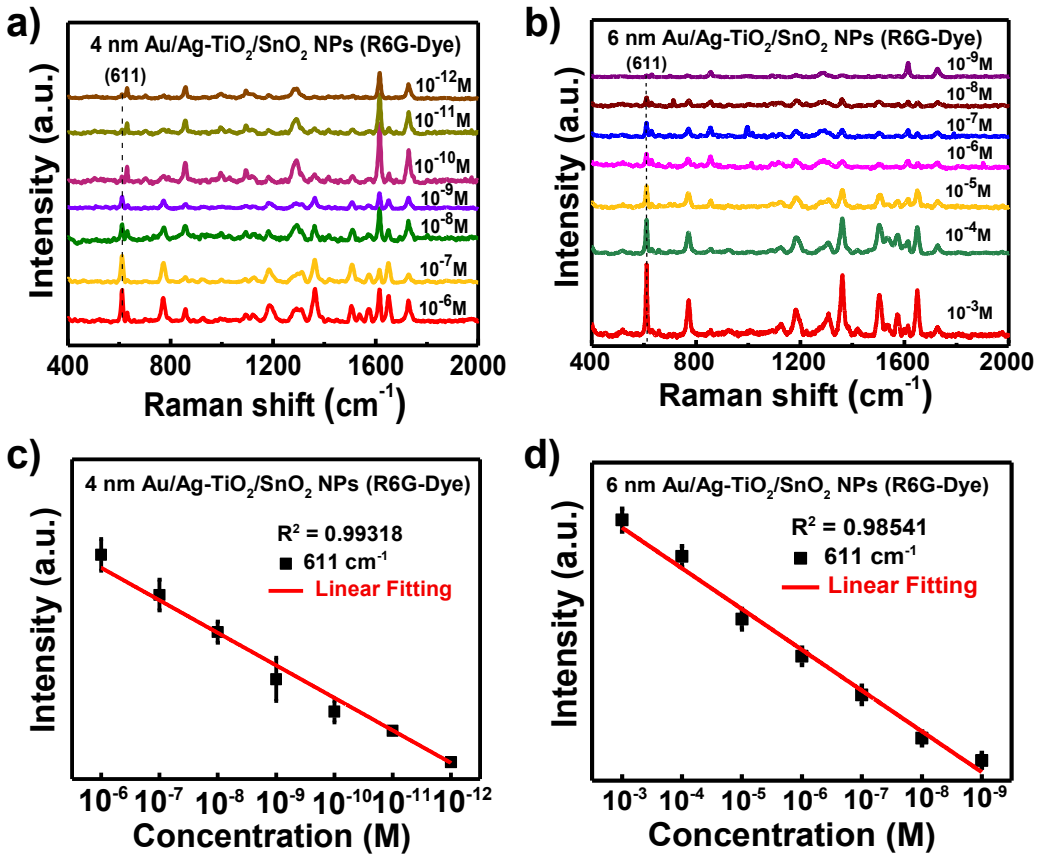

Figure 6.5 SERS spectra of R6G dye of different concentrations on **a)** 4 nm Au/Ag-TiO_2/SnO_2 NPs/plastic substrate (10^{-6} to 10^{-12} M) **b)** 6 nm Au/Ag-TiO_2/SnO_2 NPs/plastic substrate (10^{-3} to 10^{-9} M) **c)** linear fitting curve of 4 nm Au/Ag-TiO_2/SnO_2 NPs/plastic

substrate (10^{-6} to 10^{-12} M) and **d)** linear fitting curve of 6 nm Au/Ag-TiO_2/SnO_2 NPs/plastic substrate (10^{-3} to 10^{-9} M).

We have also performed a SERS study to detect vitamin B_{12} using 4 nm and 6 nm Au/Ag-TiO_2/SnO_2 NPs thin film substrates, as shown in **Figure 6.6a&b)**. The limit of detection for vitamin B_{12} adsorbed over 4 nm Au/Ag-TiO_2/SnO_2 NPs thin films and 6 nm Au/Ag-TiO_2/SnO_2 NPs thin films are found to be 10^{-9} M and 10^{-7} M, respectively, which indicates strong SERS activity at ambient temperature. The most intense peak centered at ~1501 cm^{-1} for the 4 nm thin film and 6 nm thin film (assigned to the stretching of C=C and C=N bonds of the corrins with mild contributions from CH, CH_2, and CH_3 bending modes) is preferred here for vitamin B_{12} detection. It's found that a lower SERS signal is detected as the vitamin B_{12} concentration decreases. The linear variation of peak intensity at 1501 cm^{-1} of vitamin B_{12} with concentration on the 4 nm and 6 nm thin film substrates, respectively, is displayed in **Figure 6.6c&d)**. The notable peak intensity even at a nanomolar (10^{-9} M) concentration of vitamin B_{12} on the 4 nm Au/Ag-TiO_2/SnO_2 NPs thin film substrate indicates the ultrasensitive detection, which is better than the 6 nm thin film used as a SERS substrate.

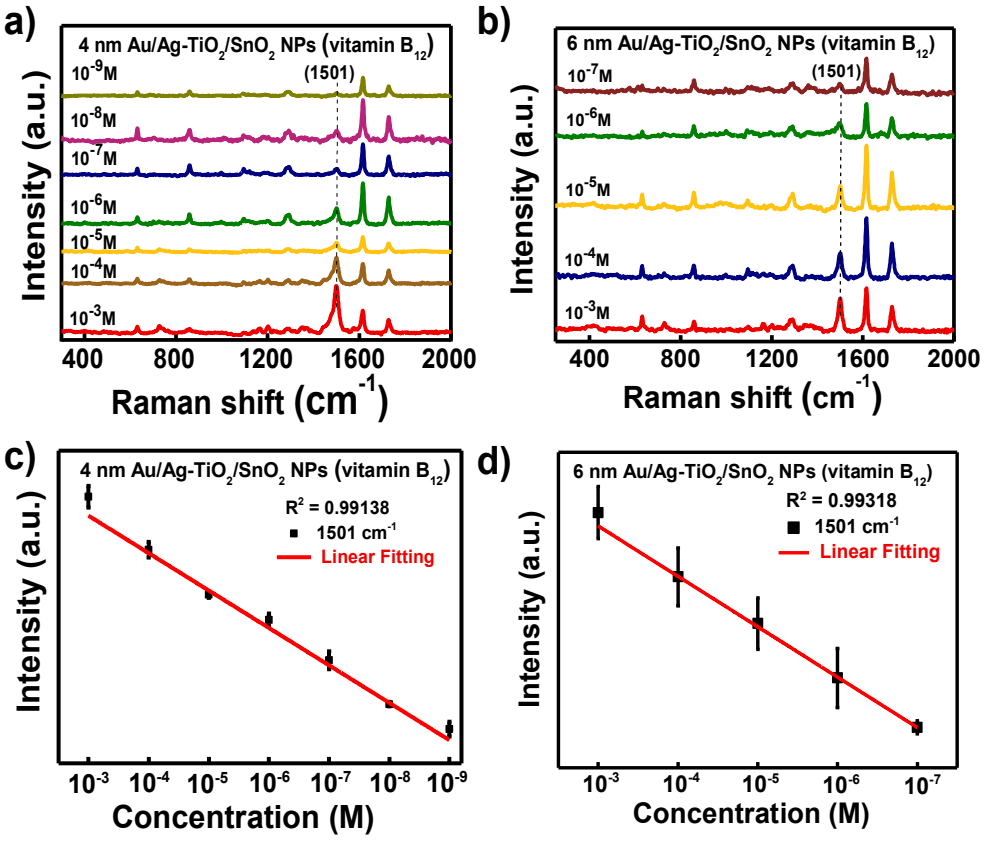

Figure 6.6 SERS spectra of vitamin B_{12} at different concentrations on **a)** 4 nm Au/Ag-TiO_2/SnO_2 NPs/plastic substrate (10^{-3} to 10^{-9} M) **b)** 6 nm Au/Ag-TiO_2/SnO_2 NPs/plastic substrate (10^{-3} to 10^{-7} M) **c)** linear fitting curve of 4 nm Au/Ag-TiO_2/SnO_2 NPs/plastic substrate (10^{-3} to 10^{-9} M) and d) linear fitting curve of 6 nm Au/Ag-TiO_2/SnO_2 NPs/plastic substrate (10^{-3} to 10^{-7} M).

To check the uniform distribution of analyte molecule molecules over SERS substrate, we have performed the SERS mapping corresponding to Raman intensity ratio of SERS substrate to analytic molecule. **Figure 6.7a&c)** shows the SERS mapping ratio or 4nm and 6nm Au/Ag-TiO_2/SnO_2 NPs corresponding to R6G dye. Additionally, the SERS uniformity is also verified by plotting the histograms showing the SERS intensity at ten different locations shown in **Figure 6.7c&d)**. The calculated coefficient of variation is ~0.017 for R6G on 4 nm Au/Ag-TiO_2/SnO_2 NPs and 0.028 for R6G on 6 nm Au/Ag-TiO_2/SnO_2 NPs. Similarly, we have performed for SERS mapping ratio corresponding vitamin B_{12} over 4nm and 6nm Au/Ag-TiO_2/SnO_2 NPs as shown in **Figure 6.8a&c)** and the histograms plot corresponding to SERS data point at ten different locations for vitamin B_{12} on 4 nm and 6nm Au/Ag-TiO_2/SnO_2 NPs as shown in **Figure 6.8b&d)**.

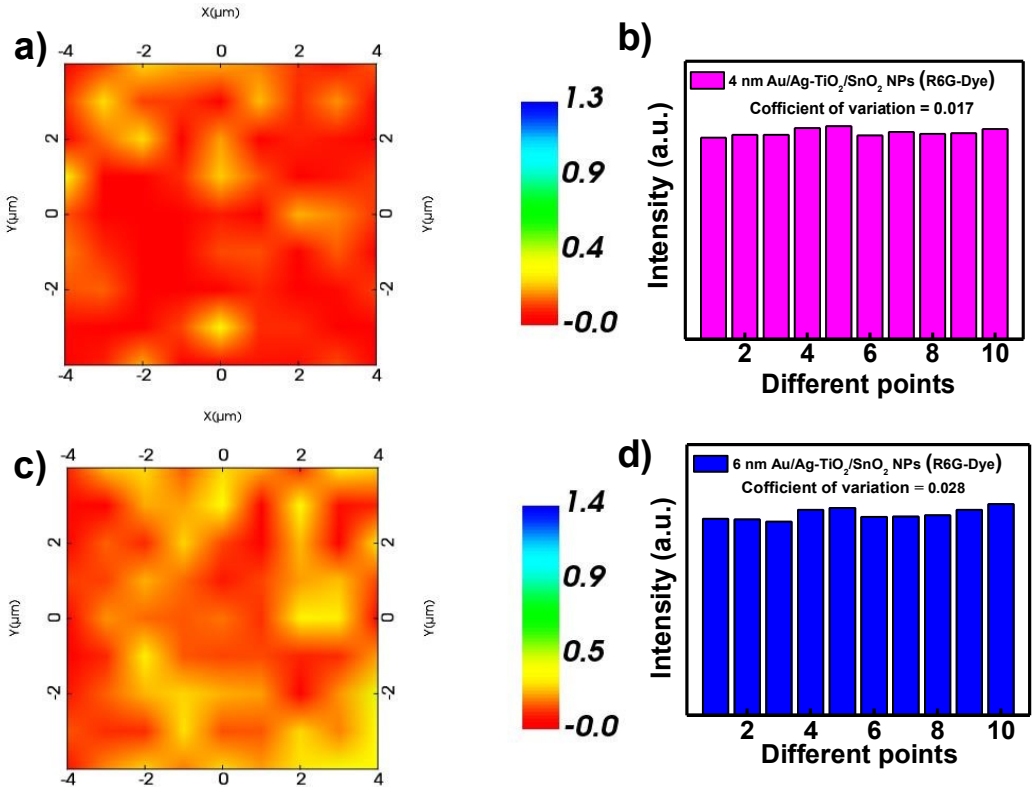

Figure 6.7 mapping images of the ratios of Raman intensities of the SERS substrate to R6G on **a)** 4 nm Au/Ag-TiO_2/SnO_2 NPs and **c)** 6 nm Au/Ag-TiO_2/SnO_2 NPs **b&d)** histograms depicting the distribution of SERS intensities at different locations for corresponding substrates, along with their coefficients of variation.

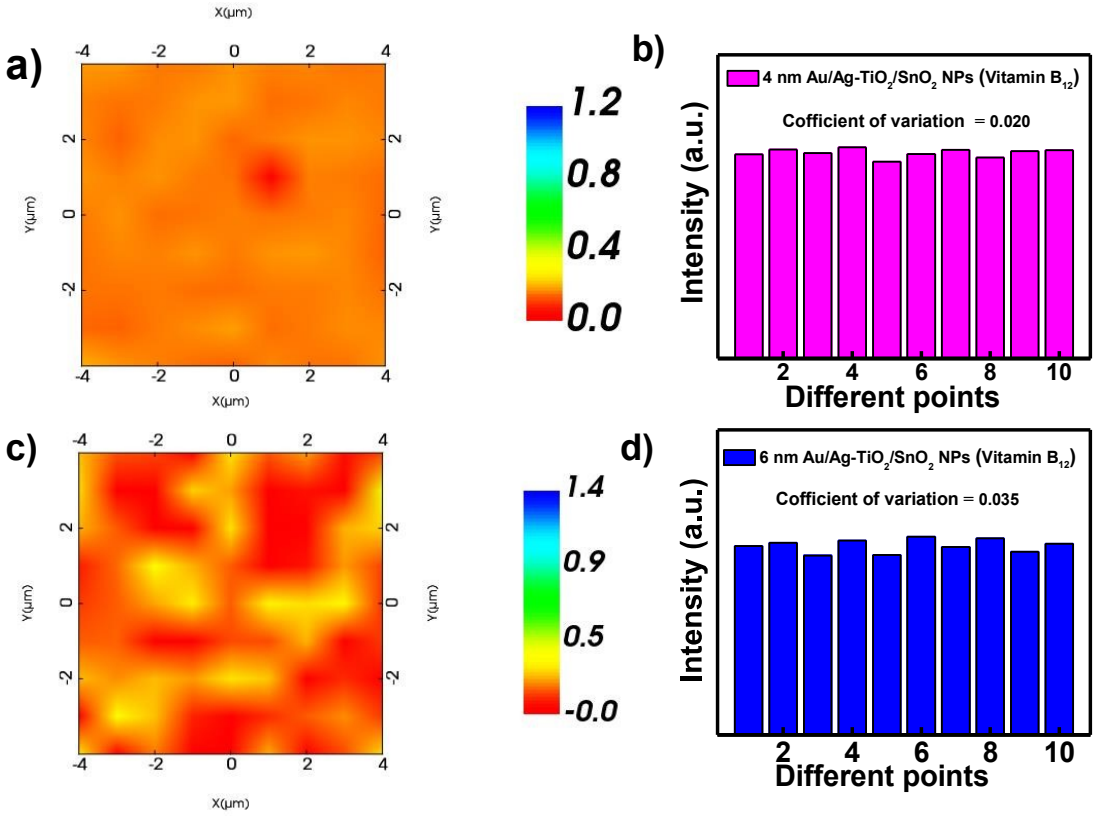

Figure 6.8 mapping images of the ratios of Raman intensities of the SERS substrate to vitamin B_{12} **a)** 4 nm Au/Ag-TiO_2/SnO_2 NPs **c)** 6 nm Au/Ag-TiO_2/SnO_2 NPs **b,d)** histograms depicting the distribution of SERS intensities at different locations for corresponding substrates, along with their coefficients of variation.

We have also performed SERS mapping at three different regions of SERS sample to check SERS uniformity throughout. The SERS ratio mapping for three different regions of R6G and vitamin B_{12} at two orders of magnitude lower than the highest detection limit is presented in **Figure 6.9** & **Figure 6.10**. This mapping clearly demonstrates the uniform distribution of these analytic molecules across both SERS substrates used for detection.

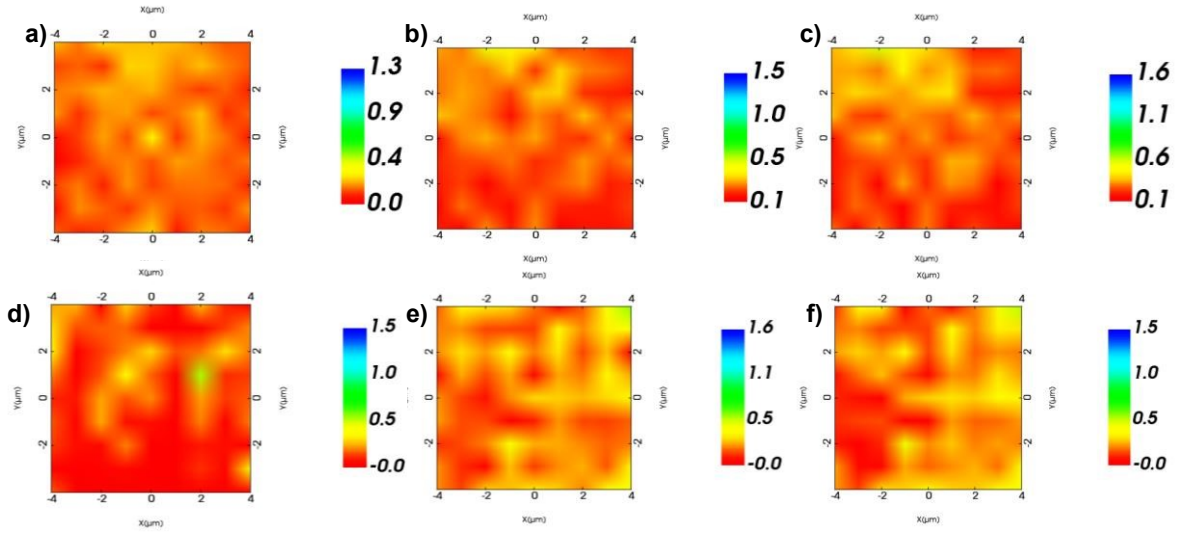

Figure 6.9 Mapping images of the ratios of Raman intensities of **a-c)** 4 nm Ag-TiO_2/SnO_2 NPs substrate to R6G and **d-f)** 6 nm Ag-TiO_2/SnO_2 NPs substrate to R6G.

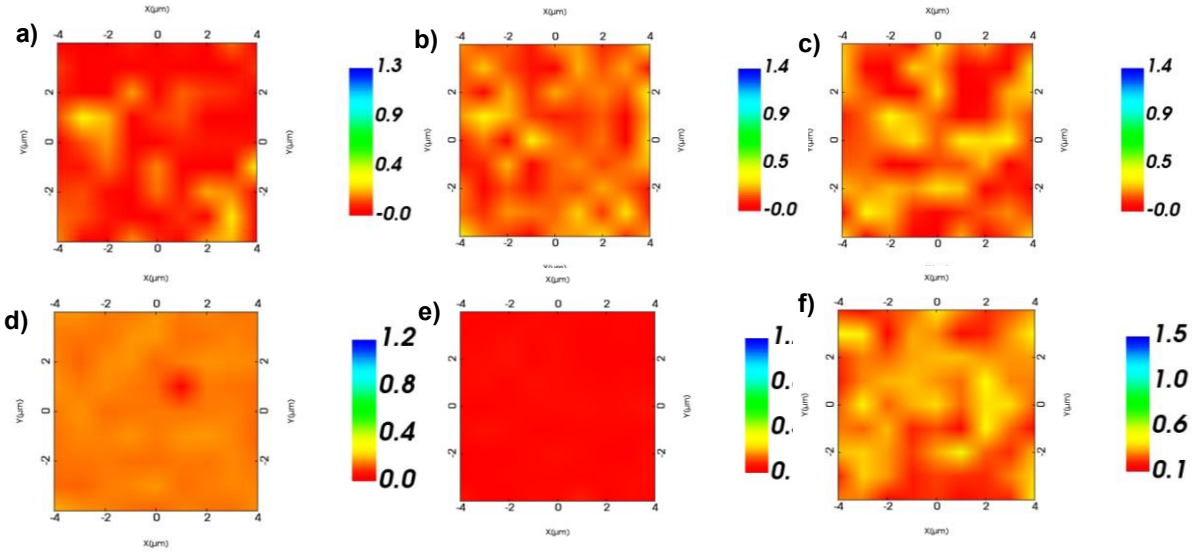

Figure 6.10 mapping images of the ratios of raman intensities of **a-c)** 4 nm Ag-TiO_2/SnO_2 NPs substrate to vitamin B_{12} and **d-f)** 6 nm Ag-TiO_2/SnO_2 NPs substrate to vitamin B_{12}.

Long-term stability of the SERS substrate is investigated at room temperature. The SERS spectra of analytes vitamin B_{12}, and R6G at the lowest detected concentration are collected after 1,2 and 3 months, as shown in **Figure 6.11a,b,c&d)**. The SERS spectra of the substrate on the 1st day and after 1,2 and 3 months show small variation, which may be due to the slight changes in measuring environments. The measured signal intensities of characteristic

peaks from the SERS substrate demonstrated the proposed substrate maintained its fine features and intensities up to months.

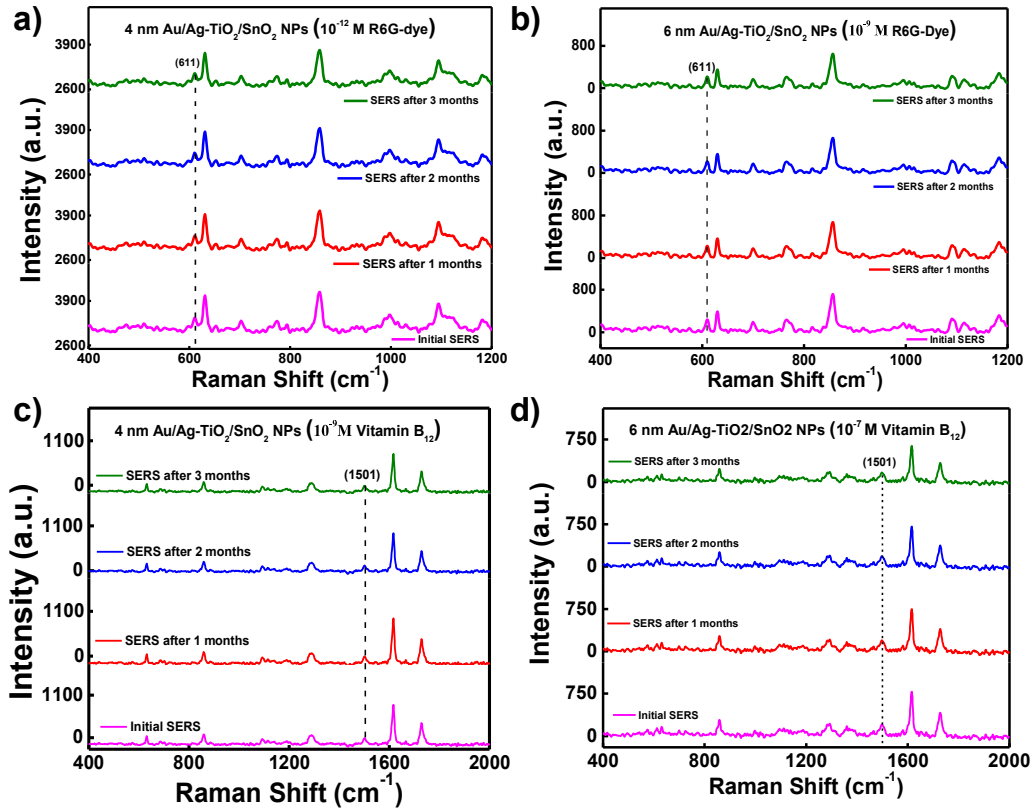

Figure 6.11 SERS spectra after 1-3 months, comparing with initial SERS initial preserved substrate **a,b)** R6G on 4 nm and 6 nm Au/Ag-TiO_2/SnO_2 and **c,d**) vitamin B_{12} on 4 nm and 6 nm Au/Ag-TiO_2/SnO_2 .

The most significant impact to SERS enhancement comes from the EM mechanism, which is predominantly due to the excitation of LSPR on the metal nanostructures. LSPR are collective oscillations of conducting electrons in the plasmonic materials, which occur when the incoming light matches the natural frequency of the outermost electrons vibrating against the restoring force of positive nuclei. When localized surface plasmons are excited, they generate intense EM fields at the surface of the nanostructures, particularly at "hot spots" such as sharp edges, tips, and interparticle junctions. The Raman scattering signal of molecules located in these hot spots is significantly enhanced due to the increased local electromagnetic field (**Figure 6.12a)**). The enhancement factor is highly dependent on the size, shape, and interparticle distance of the metal nanostructures. Optimizing these

parameters can lead to very high local field enhancements and, consequently, substantial SERS signals.[331, 332]

The other mechanism involved is chemical enhancement, wherein charge transfer (CT) between adsorbed molecules and the metal oxide semiconductor layer is considered to be crucial in plasmon driven chemical reactions. Semiconductors possess an energy gap between an empty conduction band (CB) and a full valence band (VB), and the CT between the semiconductor and molecules is dependent on the vibronic coupling of the CB or VB with the excited and ground states of the molecule. In this case, a chemical transition between the HOMO and LUMO of adsorbed molecules might take place. CT can happen from semiconductors to molecules or the other way[333] around (**Figure 6.12b)**). The key variable in the Raman scattering enhancement metal/metal oxide hybrid nanostructure (**Figure 6.12c**) is believed to be the combination of the EM mechanism (e.g., mie resonance) and chemical effects (e.g., band gap resonance). This complex enhancement mechanism includes plasmon-derived enhancement or CT from metals/metal oxide heterostructure.[334]

We used Albrecht's methods, adding Herzberg-Teller vibronic coupling into the polarizability formula, to establish an analytical expression for the Raman intensity near single or bi-metal nanoparticles. This method allows for breakdowns in the Born-Oppenheimer approximation and is extended to second order in perturbation theory. By considering the molecule-metal system as connected and including the occupied and unoccupied levels of the metal conduction band in the Herzberg-Teller expansion to improve Albrecht's estimates. We showed that the largest enhancement happens when transitions to or from the metal levels are at the energy level of Fermi by substituting an integral for the sum over metal states. The resultant polarizability (R) expression is similar to Albrecht's and can be expressed as R = A + B + C, which is the sum of three components. In this case, term A has solely Franck-Condon integrals as numerators. This factor disappears well away from resonance; nevertheless, one of the terms in A may become important close to resonance, permitting only completely symmetric Raman lines. This term is usually attributed to resonance Raman spectra. The B and C terms are Herzberg-Teller contributions resulting from metal-to-molecule or molecule-to-molecule charge-transfer transitions, respectively; these transitions "borrow" intensity from adjacent allowed molecular transitions via the

Herzberg-Teller coupling constant (h). SPR or CT processes can improve the intensity of the resultant vibrational modes, and the B and C components permit transitions to both fully symmetric and non-totally symmetric modes. The presence of any or both of the B or C factors is required when SERS spectra show intensity in non-totally symmetric normal modes.[335, 336] These components, along with the A term, may also contribute to completely symmetric bands. A term is given by-

$$\boldsymbol{R_{IC}(\omega)} = \frac{\mu_{IC}\,\mu_{IC}\,\langle i|k\rangle\langle k|f\rangle}{\{(\epsilon_1(\omega)+2\epsilon_0)^2+\epsilon_2^2(\omega)\}C\,\{(\omega_{IC}^2-\omega^2)+\Upsilon_{IC}^2)\}} \quad \text{--------- (6.1)}$$

In the denominator, the first term represents the valence band plasmon resonance, a feature present in all subsequent expressions. For the A-terms, an additional resonance occurs, which can be attributed to either the charge transfers from the HOMO to the conduction band edge (at $\omega = \omega_{IC}$) or from the valence band edge to the LUMO of the molecule (at $\omega = \omega_{VK}$). The numerator includes the oscillator strength of these charge-transfer transitions, governed by Franck- Condon selection rules, which are nonzero only for totally symmetric normal modes and allow for overtones (f = i + 1, i + 2, i + 3, ...). Consequently, when the A-term dominates, one would expect extensive progressions in totally symmetric modes. Nevertheless, such long progressions are infrequently observed in SERS spectra, indicating that the intensities of even the totally symmetric modes may result from B- or C-term contributions.[337] Both analytical formula for B and C are quite difficult since they entail infinite sums over every state of the molecule-metal system. Still, just one or a few factors will predominate in the total when the excitation wavelength is close to a CT or molecular resonance in addition to SPR. One of these dominant B terms can be expressed as:

$$\boldsymbol{R_{ICV}(\omega)} = \frac{\mu_{mol}\mu_{CT}h\,\langle i|Q_k|f\rangle}{\{(\epsilon_1(\omega)+2\epsilon_0)^2+\epsilon_2^2(\omega)\}\,\{(\omega_{mol}^2-\omega^2)+\Upsilon_{mol}^2)\}\,\{(\omega_{CT}^2-\omega^2)+\Upsilon_{CT}^2)} \text{-------- (6.2)}$$

The surface-enhanced Raman intensity is proportional to the square of the polarizability, so for a single dominant term. In this expression, i, f, and k represent the ground state, a charge-transfer state, and an excited molecular state of the molecule-metal system, respectively.

The denominator of the expression involves the sum of three terms, each representing a different resonance contribution to SERS. This shows how various resonant interactions, including CT and molecular resonances, in conjunction with SPR, contribute to the enhanced Raman signal.

Apart from the metals to semiconductors CT pathway, photosensitive molecules may also facilitate the reverse direction of CT from semiconductors to metals. In these situations, depending on how the building blocks and SERS probes are assembled, CT either begins with the semiconductors or the adsorbed molecules.[338] In the case of Au/Ag-TiO_2/SnO_2 NPs grown over the plastic substrate, used analytic molecules R6G & B_{12} (HOMO levels are -5.7, -5.5 eV, LUMO levels are -3.4, -3.5 eV respectively) are expected to lie as per literature reports.[339] For both analytic molecules, electrons are first excited from the HOMO level to the LUMO level (**Figure 6.12d&e)**), then subsequently transferred to lower level of the Ag-TiO_2/SnO_2 NPs complex due to the energy level equilibration (band position of semiconductor are collected from literature review) and then injected into the Fermi levels of Au (W_f~ -5.1 eV) via the Ag NPs (W_f~ -4.7 eV).[294, 295, 324] The introduction of bi-metallic Au-Ag NPs, decreased the CT threshold, extended the CT response to NIR region, and enhanced the CT efficiency in the high-energy region.

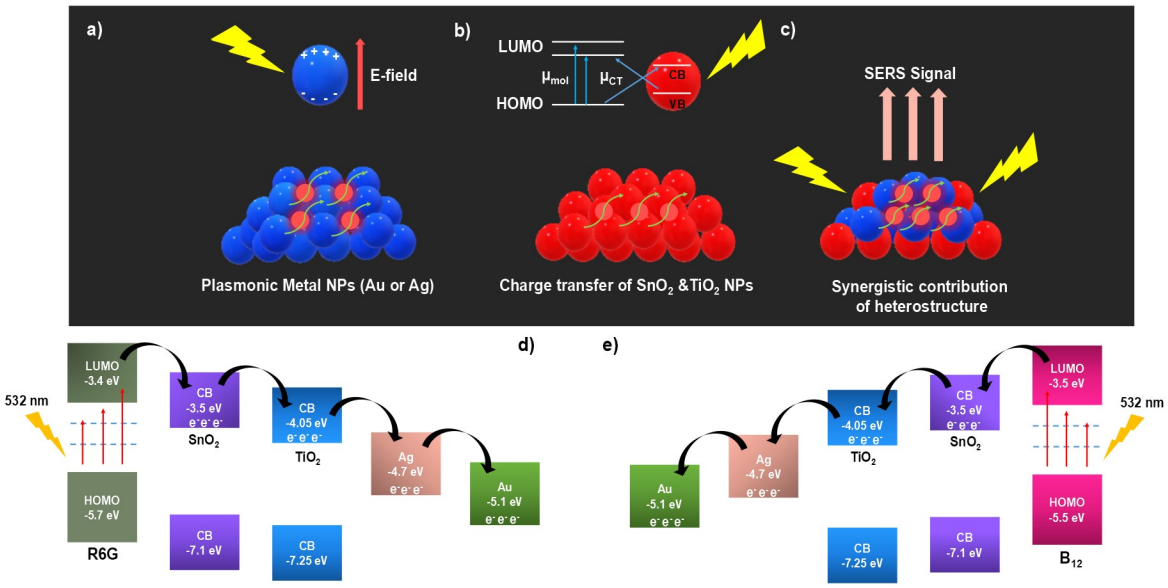

Figure 6.12a,b&c) SERS mechanisms: plasmon-induced enhancement on metals, CT on semiconductors, and the synergistic contribution of plasmons and CT on metal–semiconductor heterostructures. Mechanisms of the photo induced CT process in Au-Ag based metal–semiconductor heterostructures: **d&e)** Au/Ag-TiO_2/SnO_2 NPs heterostructures for R6G dye and vitamin B_{12} respectively.

For further investigations of CT mechanism, we examined the change in the ambient temperature PL spectrum of (4 or 6 nm Au)/Ag-TiO_2/SnO_2 NPs on plastic substrates with and without R6G dye & vitamin B_{12} biomolecules (**Figure 6.13a&b)**). Ambient temperature PL spectra and its quenching for R6G dye demonstrate that the PL intensities of substrates treated with the dye (10^{-3} M) decreased drastically (~ 60–70%) when compared to the PL intensities of the same SERS substrates without the dye. In case of vitamin B_{12} (10^{-3} M) PL almost quenched completely compared to the original substrate. This experiment demonstrates that the CT process has been confirmed since the greatest number of electrons are transported from SERS substrates to R6G dye and vitamin B_{12} biomolecules, and only a small number of electrons return from the CB to the VB.

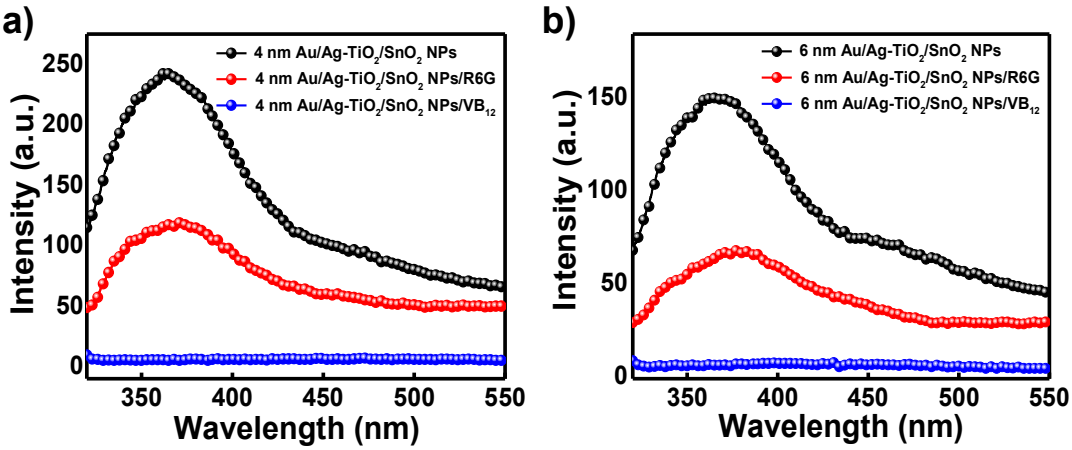

Figure 6.13 PL spectra of **a)** 4 nm Au/Ag-TiO_2/SnO_2 NPs and **b)** 6 nm Au/Ag-TiO_2/SnO_2 NPs on plastic substrate with and without R6G dye & vitamin B_{12}.

Additionally, we have determined the number of biomolecules involved in SERS as well as in normal Raman scattering N_{SERS} and N_{Raman} respectively. Using this calculation, we further estimated the SERS enhancement factor (EF) by using the following equations:

$$N_{Raman} = \frac{CVN_A A_{Raman}}{A_{Sub}} \qquad \text{--------- (6.3)}$$

$$N_{SERS} = \frac{\rho h N_A A_{Raman}}{M} \qquad \text{--------- (6.4)}$$

$$\mathbf{EF} = \frac{I_{SERS}\, N_{Raman}}{I_{Raman}\, N_{SERS}} \qquad \text{--------- (6.5)}$$

Here, C denotes the molar concentration of the biomolecule in solution, V is the volume of the irradiated solution, and N_A is Avogadro number. The laser spot area is denoted by A_{Raman} , while A_{sub} represents the effective area of the substrate. The density and molecular weight of the bulk biomolecule are indicated by ρ and M, respectively. I_{SERS} represents the intensity of the Raman signal obtained with the SERS substrate, while I_{Raman} is the intensity of the normal Raman signal recorded without any enhancement. N_{Raman} refers to the number of molecules contributing to the normal Raman signal and N_{SERS} indicates the number of molecules interacting directly with the SERS-active surface, usually limited to those located at or near the substrate's hot spots.

In the SERS studies, 1 and 116 molecules for R6G are detected on 4 nm and 6nm Au/Ag-TiO_2/SnO_2 NPs at the lowest concentrations of 10^{-12} M and 10^{-9} M, respectively. For vitamin B_{12}, 89 and 6120 molecules are detected on 4 nm and 6 nm Au/Ag- TiO_2/SnO_2 NPs substrates at 10^{-9} M and 10^{-7} M, respectively. After calculating and substituting all parameters into **Equation 6.5**, the EF values for R6G at ~ 611 cm^{-1}, and vitamin B_{12} at ~1501 cm^{-1} on the 4 nm Au/Ag-TiO_2/SnO_2 NPs substrate are found to be 3.4 $\times 10^8$ and 2.2 $\times 10^5$, respectively. Similarly, for the 6 nm Au/Ag-TiO_2/SnO_2 NPs substrate, the EF values are 4.8 $\times 10^5$ for R6G and for vitamin B_{12} 5.1$\times 10^3$. The calculated number of molecules, and EF are provided in **Table 6.1** and **Table 6.2**.

Table 6.1 Calculated No. of Molecules for SERS Substrate

Substrates	R6G	Vitamin B_{12}
4 nm Au/Ag-TiO_2/SnO_2 NPs	1	89
6 nm Au/Ag-TiO_2/SnO_2 NPs	116	6120

Table 6.2 Calculated EF for SERS Substrate

Substrates	R6G	Vitamin B_{12}
4 nm Au/Ag-TiO_2/SnO_2 NPs	2.07×10^8	2.2×10^5
6 nm Au/Ag-TiO_2/SnO_2 NPs	6.024×10^5	6.38×10^3

Table 6.3 presents a comparison of detection limits for different analytes on various SERS substrates reported in literature. The detection limits achieved in this study notably surpass those reported for pristine metal/metal oxide substrates.

Table 6.3 Comparison Table of SERS Detection Limits for Different Substrates with Different Analytical Methods

SERS Substrate	Preparation Method	Detection method	Analyte molecules	Detection limit (M)	Ref.
MoS_2@ZnO@Ag	Hydrothermal	SERS	Bilirubin	10^{-8}	[340]
Ag@Fe_2O_3	Hydrothermal	SERS	R6G	9.3×10^{-10}	[341]
			Bilirubin	2.3×10^{-8}	
Ag/SnO_2 nanocore composite/glass	Spray-pyrolysis/PVD	SERS	R6G	10^{-12}	[342]
Au/SnO_2/glass	PVD	SERS	Ciprofloxacin (CIP)	10^{-8}	[294]
10 nm Ag/$Ag_4Ti_5O_{12}$ /glass	Chemical method/PVD	SERS	MB	10^{-9}	[343]
Ag@SiO_2-Au NPs	Chemical Method	SERS	RhB	5×10^{-9}	[344]
4 nm Au/Ag-TiO_2 /plastic	**Chemical method/PVD**	**SERS**	**R6G**	**10^{-12}**	**This work**
			Vitamin B_{12}	**10^{-9}**	

6.4 Conclusion

In summary, we have successfully synthesized nano-porous Au-Ag bi-metallic thin film on a pre-deposited solution processed Ag-TiO_2/SnO_2 NPs film of different mass thickness of Au NPs and used them as SERS substrates for detecting different analytes like R6G dye and

vitamin B_{12} biomolecules. Morphological study shows the 4 nm Au/Ag-TiO_2/SnO_2 NPs/plastic sample has a percolated metallic nanostructure that has high porosity with high surface roughness but uniformly distributed throughout the sample. This typical Au-Ag nanostructure has high environmental stability due to its typical Au-embedded Ag nanostructure, also has high density EM hotspots originating from its nanoporous structure and high roughness which is an essential condition for developing a highly sensitive SERS substrate. Besides, Au-Ag nanostructure is grown inside TiO_2 matrix that helps charge transfer of plasmon induced hot electrons from Au-Au nanostructure to TiO_2, which can enhance the SERS sensitivity. The SERS detection limits of R6G dye on 4 or 6 nm Au/Ag-TiO_2/SnO_2 NPs/plastic substrates are 10^{-12} & 10^{-9} with EF values of 2.07×10^8 and 6.02×10^5 respectively. While SERS detection limits of vitamin B_{12} on 4 or 6 nm Au/Ag-TiO_2/SnO_2 NPs/plastic substrates are 10^{-9} & 10^{-7} M with EF values of 2.2×10^5 and 6.38×10^3 respectively. These superior SERS performances of Au-Ag thin films are due to strong coupling of LSPR effect of plasmonic metal NPs with molecular resonance & CT process from metal/metal oxide layer to analytic molecule and this CT mechanism is verified by observing the decline of ambient temperature PL of R6G dye & vitamin B_{12} molecule adsorbed SERS substrates.